Spotlight SAR Data Focusing Based on a Two-Step Processing Approach

Riccardo Lanari, *Senior Member, IEEE,* Manlio Tesauro, Eugenio Sansosti, *Member, IEEE,* and Gianfranco Fornaro

***Abstract*—We present a new spotlight SAR data-focusing algorithm based on a two-step processing strategy that combines the advantages of two commonly adopted processing approaches: the efficiency of SPECAN algorithms and the precision of stripmap focusing techniques. The first step of the proposed algorithm implements a linear and space-invariant azimuth filtering that is carried out via a deramping-based technique representing a simplified version of the SPECAN approach. This operation allows us to perform a bulk azimuth raw data compression and to achieve a pixel spacing smaller than (or equal to) the expected azimuth resolution of the fully focused image. Thus, the azimuth spectral folding phenomenon, typically affecting the spotlight data, is overcome, and the space-variant characteristics of the stripmap system transfer function are preserved. Accordingly, the residual and precise focusing of the SAR data is achieved by applying a conventional stripmap processing procedure requiring a minor modification and implemented in the frequency domain. The extension of the proposed technique to the case of high bandwidth transmitted chirp signals is also discussed.**

Experiments carried out on real and simulated data confirm the validity of the presented approach, which is mainly focused on spaceborne systems.

***Index Terms*—Raw data focusing, spectral analysis (SPECAN) processing algorithms.**

I. Introduction

SYNTHETIC aperture radar (SAR) spotlight mode allows the generation of microwave images with high geometric resolutions [1], [2]. This result is achieved by steering the radar antenna beam, during the raw data acquisition interval, to always illuminate the same area on the ground (*spot*). Accordingly, from each target located in the lighted area, a large number of backscattered echoes is received, and their coherent combination allows to obtain the required azimuth resolution. Similarly, high resolution in the range direction is achieved by transmitting a high bandwidth chirp followed by a further data processing on each received echo.

The first algorithms proposed for spotlight raw data processing are based on the similarity between spotlight SAR systems and computer tomography: they are usually referred to as polar format and convolution backprojection techniques [3]–[5]. The former are computationally efficient but request a nontrivial interpolation step from a polar to rectangular grid: the image quality can be therefore affected by uncompensated range curvature effects [6] and interpolation errors. The latter allow overcoming these limitations but are generally inefficient if implementations on dedicated architectures are not considered [5].

Most recently, the development of spotlight raw data processing algorithms based on stripmap mode focusing techniques operating in the frequency domain has received increasing interest [7]–[10]. Indeed, strip-mode processing procedures that are precise, efficient, and requiring less stringent approximations (compared to those involved in the tomographic approaches) are available [11]–[13]. However, a relevant limitation to the straightforward application of these techniques to the spotlight data processing is represented by the fact that the raw signal azimuth bandwidth is, in the spotlight case, generally greater (often much greater) than the azimuth sampling frequency, referred to as pulse repetition frequency (prf). As a consequence, data processing carried out in the Fourier domain, as that involved in efficient strip-mode focusing, cannot be directly implemented on the full aperture because of the consequential azimuth spectrum folding effect.

A way to overcome this limitation is based on partitioning the received signal into azimuth blocks whose block-bandwidths are smaller than the sampling frequency. Standard strip mode focusing techniques are then applied to each data block and the processed signals are then combined to generate the fully-resolved spotlight image [9], [10]. Completely different processing solutions, based on a nontrivial reconstruction of the unfolded azimuth spectrum from the folded one associated to the raw signal, are also available [7], [8].

On the other hand, a relatively simple spotlight processing algorithm can be implemented by applying the spectral analysis (SPECAN) technique [14]. In this case, the received raw data are azimuth focused via the application of a deramping function (a multiplication by a properly chosen chirp signal) followed by a final azimuth FT operation. The azimuth deramping factor is updated in range to allow for the compensation of the space-varying characteristic of the received data due to the (azimuth) chirp rate range variation (focus depth). This procedure is attractive as far as computational efficiency and capability to overcome the azimuth spectral folding effect are concerned. However, its main limitation is represented by the lack of a precise range cell migration (RCM) compensation that is often relevant in spotlight mode SAR systems due to high resolution requirements.

Manuscript received March 30, 2000; revised November 29, 2000. This work was partially supported by the Italian Space Agency, Roma, Italy. The spotlight SIR-C data have been processed at the Jet Propulsion Laboratory, Pasadena, CA.

R. Lanari, E. Sansosti, and G. Fornaro are with the Istituto di Ricerca per l'Elettromagnetismo e i Componenti Elettronici (IRECE) 328 I-80124 Napoli, Italy, (e-mail: lanari@irece.na.cnr.it; sansosti@irece.na.cnr.it; fornaro@irece.na.cnr.it).

M. Tesauro is with the Dipartimento di Ingegneria dell'Innovazione, Università degli Studi di Lecce, I-73100 Lecce, Italy (e-mail: manlio.tesauro@unile.it).

Publisher Item Identifier S 0196-2892(01)07625-2.

In this paper, we propose an alternative spotlight data focusing technique based on decoupling the overall focusing operation in two main steps. The key point of the proposed approach is to combine the advantages of efficient SPECAN and precise stripmap focusing approaches. In particular, the first processing step carries out a filtering operation aimed to achieve a *bulk* azimuth raw data compression and an output pixel spacing smaller than (or equal to) the expected final azimuth resolution. Similar to SPECAN processing algorithms, this filtering operation is efficiently carried out via a deramping-based approach [14] but, at variance of the former, the chirp rate of the deramping function is kept constant and properly fixed at a *convenient* value. This is a key point in the proposed processing procedure that allows preserving the space variant characteristic of the residual system transfer function (STF). A discussion on the impact of the chirp rate selection on possible artifacts that may appear at the image borders is also provided.

The second processing step carries out the residual focusing of the data via the use of a conventional stripmap processing procedure implemented in the frequency domain and requiring only minor modifications in the available codes. This spectral domain focusing operation is now possible because, following the bulk azimuth compression, the folding effect of the raw signal azimuth spectrum has been totally overcome. More precisely, this second (residual) processing step performs the precise RCM compensation, the data range compression and the residual azimuth data compression; the latter accounts for higher order terms not compensated in the bulk azimuth processing step. The minor modifications to be performed in available stripmap processing codes are essentially a change of the azimuth filter function, which accounts for the already compensated quadratic azimuth phase term, and a change in the azimuth pixel spacing of the input data.

It is worth noting the role that the bulk azimuth compression operation plays in our approach to a preprocessing step that extends the processing capability of conventional stripmap focusing procedures to spotlight data. In addition, the proposed processing algorithm does not require a specific manipulation and/or interpolation of the data, such as those necessary in azimuth block divisions or in unfolded signal spectrum reconstruction-based algorithms. Accordingly, we have finally achieved a processing procedure that is simple, precise and computationally efficient because it does not imply any significant increase of the raw data matrix dimensions and only includes fast Fourier transforms (FFTs) and matrix multiplication. Moreover, it can be easily extended to the case of high bandwidth transmitted signals wherein spectral folding effects could appear in the range direction as well. In our case, the implemented solution is based again on a deramping approach, that is, at variance of conventional focusing techniques performed following the A/D conversion rather than before. A number of experiments carried out on a simulated and a real data set, the latter acquired by the experimental C-band sensor of the SIR-C system during the SIR-C/X-SAR mission in 1994 [9], demonstrate the validity of the presented approach.

As a final remark, we want to stress that the presented analysis is focused on spaceborne systems typically characterized by small squint angles [15] during the acquisition (often less than 1°) and negligible platform motion errors. However, the extension of the proposed algorithm to the airborne case is certainly possible but, in this case, additional and specific issues such as motion compensation and/or high squint angle values in the data acquisition must be carefully considered. This is worth for future analysis.

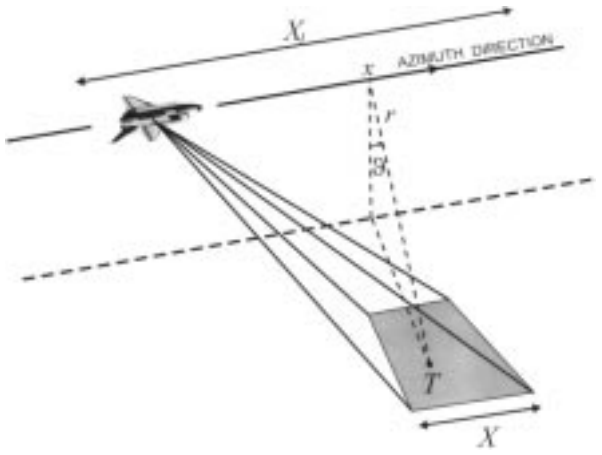

Fig. 1. Spotlight system geometry.

II. Frequency Domain Analysis

Let us start the analysis by considering the spotlight geometry of Fig. 1, where the cylindrical coordinate system (x, r, ϑ) is shown. The x-axis, assumed coincident with the platform flight path, is referred to as azimuth direction r and ϑ are the (closest approach) target range and look angle, respectively.[1]

We assume in the following that the sensor, mounted onboard a platform moving at the constant velocity $\mathbf{v} = v\hat{\mathbf{x}}$, transmits, at times $t_n - \tau/2$, the following linear frequency modulated (chirp) pulses:

$$f_1(t - t_n) = \exp(j\omega t)\exp\left[-j\,\frac{\alpha}{2}\,(t - t_n)^2\right]\operatorname{rect}\left[\frac{t - t_n}{\tau}\right] \tag{1}$$

where

t	continuous time variable;
ω	angular carrier frequency;
τ	pulse duration;
$\alpha/2\pi \approx \Delta f/\tau$	chirp rate, being Δf the transmitted signal bandwidth.

We also assume that λ is the system wavelength, X_I the trajectory flight portion used to acquire the raw data (see Fig. 1), and $w^2[x, r] \approx \operatorname{rect}[x/X]$, the two-way antenna pattern factor, and $X = \lambda r/L$ is the illuminated area (spot) with L being the azimuth dimension of the real, onboard antenna. Note that the assumed simplification on $w^2[\cdot]$ allows avoiding the antenna footprint dependence on the platform location whose impact is

[1]Note that we have assumed the platform trajectory to be a straight line which is appropriate for airborne but not for spaceborne sensors. However, it can be shown that spaceborne data can be processed in the same manner as airborne data if the closed approach distance and the azimuth velocity are properly considered [16] or, more precisely, via the appropriate sensor-target distance evaluation [17].

inessential for the following analysis. A more detailed discussion on this matter can be found in [10].

Let us now consider a point target $T \equiv (x, r, \vartheta)$ located within the illuminated spot, the signal backscattered by T and received onboard is represented, after the heterodyne process [that removes the fast varying term $\exp(j\omega t)$], by[2]

$$\begin{aligned} f(x'-x, r'-r, x, r) &= \exp\left(-j\omega\frac{2R}{c}\right)\exp\left[-j\frac{\alpha}{2}\left(t-t_n-\frac{2R}{c}\right)^2\right] \\ &\quad\times \operatorname{rect}\left[\frac{t-t_n-2R/c}{\tau}\right]\operatorname{rect}\left[\frac{x'}{X_I}\right]\operatorname{rect}\left[\frac{x}{X}\right] \\ &= \exp\left(-j\frac{4\pi}{\lambda}r\right)\exp\left[-j\frac{2\alpha}{c^2}(r'-r-\Delta R)^2\right] \\ &\quad\times \operatorname{rect}\left[\frac{r'-r-\Delta R}{c\tau/2}\right]\exp\left[-j\frac{4\pi}{\lambda}\Delta R\right] \\ &\quad\times \operatorname{rect}\left[\frac{x'}{X_I}\right]\operatorname{rect}\left[\frac{x}{X}\right] \\ &= \exp\left(-j\frac{4\pi}{\lambda}r\right)b[r'-r-\Delta R]a(x'-x, x, r). \end{aligned} \tag{2}$$

In (2), we have introduced the spatial variable $r' = c(t-t_n)/2$, $x' = vt_n$ is the sensor azimuth coordinate

$$R = \sqrt{r^2+(x'-x)^2} = r + \Delta R \tag{3}$$

is the sensor-target distance, and we assumed

$$\begin{aligned} b[r'-r-\Delta R] &= \exp\left[-j\frac{2\alpha}{c^2}(r'-r-\Delta R)^2\right]\operatorname{rect}\left[\frac{r'-r-\Delta R}{c\tau/2}\right] \end{aligned} \tag{4a}$$

$$\begin{aligned} a(x'-x, x, r) &= \exp\left[-j\frac{4\pi}{\lambda}\Delta R\right]\operatorname{rect}\left[\frac{x'}{X_I}\right]\operatorname{rect}\left[\frac{x}{X}\right]. \end{aligned} \tag{4b}$$

Because this preliminary analysis is focused on the evaluation of the raw signal azimuth spectrum, let us consider the simplified expression of (4b)

$$a(x'-x, x, r) \approx \exp\left[-j2\pi\frac{(x'-x)^2}{\lambda r}\right]\operatorname{rect}\left[\frac{x'}{X_I}\right]\operatorname{rect}\left[\frac{x}{X}\right] \tag{5}$$

wherein

$$\Delta R \approx \frac{(x'-x)^2}{2r}. \tag{6}$$

Note that higher order terms in the approximation in (6) are accounted for during the subsequent precision focusing. Moreover, let us also neglect the range curvature effect, highlighted by the factor ΔR in (4a), which is inessential for the following azimuth bandwidth evaluation [15].

[2]Inessential amplitude factors are hereafter neglected.

By using the stationary phase method (SPM), it follows that

$$\begin{aligned} A[\xi, x, r] &= \mathrm{FT}[a(x'-x, x, r)] \\ &= \int a(x'-x, x, r)\exp(-j2\pi\xi x')\,dx' \\ &\sim \exp\left[j2\pi\left(\xi^2\frac{\lambda r}{4}-\xi x\right)\right]\operatorname{rect}\left[\frac{\xi-\frac{2x}{\lambda r}}{\frac{2}{L}\frac{X_I}{X}}\right] \\ &\quad\times \operatorname{rect}\left[\frac{x}{X}\right] \end{aligned} \tag{7}$$

wherein FT[.] represents the Fourier transform operator, and ξ is the azimuth (spatial) frequency. Equation (7) shows that the azimuth spectrum is centered on the frequency $2x/(\lambda r)$ and that the signal bandwidth is $(X_I/X)(2/L)$, i.e., it is increased by the factor $X_I/X > 1$ with respect to the strip mode case, for which it would be $2/L$ [15]. This bandwidth increase is responsible for the azimuth resolution improvement achieved in the spotlight case.

The previous analysis has been focused on the azimuth signal component backscattered by a single target. Should we consider an extended scene, the total signal bandwidth, for example $\Delta\xi$, could be easily computed from (7) by accounting for the azimuth spot extension X. In this case, we get

$$\Delta\xi \approx \frac{2}{L}\frac{X_I+X}{X}. \tag{8}$$

Since the maximum value of $\Delta\xi$ is of interest, the minimum value of X, i.e., that relative to the nearest range, should be considered. This is assumed hereafter, although we underline that in the spotlight case, due to the typically limited range extension of the illuminated spot, the range dependence of X has, generally, a negligible effect.

The previous analysis does not account for the effect of the sampling operation that is carried out on the received signal. In this case it is evident from (8) that the azimuth (spatial) sampling frequency, say ξ_S, should be increased, with respect to the strip case, at least by the following factor:

$$V = \frac{\Delta\xi}{2/L} \approx \frac{(X_I+X)}{X} \tag{9}$$

in order to avoid any azimuth spectral folding effect [18]. On the other hand, this sampling frequency increase would lead to large data rates and could generate severe range ambiguity problems [15]. Accordingly, the values of ξ_S are typically kept as those of strip-mode acquisition. An azimuth spectral folding is therefore generated. This effect prevents the straightforward application of conventional stripmap focusing techniques implemented in the frequency domain.

An additional consideration on (9) is in order. Let us assume that $\Delta x' = L/2$ and $\Delta x'' = 1/\Delta\xi$ are the raw data and the focused image azimuth pixel dimensions, respectively, the latter chosen in agreement with the Nyquist limit available from (8). In this case, we get from (9)

$$\frac{X}{\Delta x''} \approx \frac{(X_I+X)}{\Delta x'}. \tag{10}$$

Equation (10) clarifies that the azimuth number of pixel in the raw data set and in the focused image, i.e., $X_I/\Delta x'$ and $X/\Delta x''$, respectively, are comparable, and they become closer as X_I increases with respect to the azimuth antenna footprint X.

III. Bulk Azimuth Raw Data Compression

Let us now investigate a possible solution to the azimuth spectral folding effect discussed in the previous section. The proposed approach is based on a linear and space-invariant azimuth filtering operation that performs a bulk azimuth data compression and achieves an output pixel spacing, satisfying the Nyquist limit shown in (8). This operation is efficiently implemented without any large zero padding step, via a deramping-based technique [1], [2], [14].

A. Continuous Domain Analysis

Key point of the presented technique is the azimuth convolution between the raw data and the quadratic phase signal

$$s(x') = \exp\left[j2\pi \frac{x'^2}{\lambda \tilde{r}}\right], \quad \text{with } r_m \le \tilde{r} \le r_M \tag{11}$$

wherein r_m and r_M are the nearest and the farthest ranges of the illuminated spot, respectively, and $\tilde{r}$ represents the range value of a generic point target located within the spot. No specific assumption has yet been made on the factor $\tilde{r}$ in (11), although we anticipate that the impact of any particular selection for this term is later discussed in detail. We also underline that the raw signal range component, accounting for the range independent (RI) and range dependent (RD) RCM effects, is neglected in the azimuth convolution operation presented in this section. All these components are restored and accounted for during the subsequent and highly precise second processing step.

The azimuth convolution between the signal $a(\cdot)$ in (5), for the case of an isolated target, and the function $s(\cdot)$ in (11) gives

$$\begin{aligned}
\overline{a}(x', x, r) &= a(x' - x, x, r) \otimes_{\text{az}} s(x') \\
&= \exp\left[j2\pi \frac{(x')^2}{\lambda \tilde{r}}\right] \int a(z - x, x, r) \\
&\quad \times \exp\left[j2\pi \frac{z^2}{\lambda \tilde{r}}\right] \exp\left[j2\pi \frac{2x'}{\lambda \tilde{r}} z\right] dz \\
&= \text{rect}\left[\frac{x}{X}\right] \int \text{rect}\left[\frac{z}{X_I}\right] \exp\left[-j2\pi \frac{(z-x)^2}{\lambda r}\right] \\
&\quad \times \exp\left[j2\pi \frac{(x'-z)^2}{\lambda \tilde{r}}\right] dz \\
&= \text{rect}\left[\frac{x}{X}\right] \exp\left[j\frac{2\pi}{\lambda}\left(\frac{x'^2}{\tilde{r}} - \frac{x^2}{r}\right)\right] \\
&\quad \times \int \text{rect}\left[\frac{z}{X_I}\right] \exp\left[-j\frac{2\pi}{\lambda \tilde{r}} \frac{r - \tilde{r}}{r} z^2\right] \\
&\quad \times \exp\left[-j\frac{4\pi}{\lambda}\left(\frac{x'}{\tilde{r}} - \frac{x}{r}\right) z\right] dz
\end{aligned} \tag{12}$$

wherein the symbol $\otimes_{\text{az}}$ represents the azimuth convolution operation. Equation (12) shows that the result of the convolution depends on the range location r of the target and on the value of $\tilde{r}$. The second line in (12) shows that this azimuth convolution is essentially a deramping based (SPECAN) processing, involving a chirp multiplication of the azimuth signal, a subsequent FT and a residual phase cancellation. Indeed, but for the above mentioned approximations, this processing step allows us to achieve an azimuth compression which is *full* only for those targets located at $r = \tilde{r}$. This point can be clarified by reconsidering (12). Indeed, if we assume $|r - \tilde{r}|/r = 0$ and neglect inessential constant amplitude factors, (12) can be rewritten as follows:

$$\begin{aligned}
\overline{a}(x', x, r) = \text{rect}\left[\frac{x}{X}\right] \text{sinc}\left[\frac{2\pi}{L} \frac{X_I}{X} (x' - x)\right] \\
\times \exp\left[j2\pi \frac{x'^2 - x^2}{\lambda r}\right]
\end{aligned} \tag{13}$$

wherein the imaged target is fully azimuth focused.

For any r and $\tilde{r}$ with $\tilde{r} \neq r$, by assuming the validity of the SPM method[3] we get

$$\begin{aligned}
\overline{a}(x', x, r) \sim \text{rect}\left[\frac{x}{X}\right] \text{rect}\left[\frac{x' - x\frac{\tilde{r}}{r}}{X_I |r - \tilde{r}|/r}\right] \\
\times \exp\left[-j2\pi \frac{(x' - x)^2}{\lambda (r - \tilde{r})}\right].
\end{aligned} \tag{14}$$

The worst case is represented by $|r - \tilde{r}|/r = |r_m - r_M|/r_m$, for which the resulting signal is centered around $x r_M/r_m$ and extends for $X_I |r_M - r_m|/r_m$. However, because the range extension of the spot area is typically very small, we can assume $|r_M - r_m|/r_m \ll 1$. Accordingly, $X_I |r_M - r_m|/r_m \ll X_I$ and, even in this limiting case, a compression effect, although partial with respect to that achieved in (13), is obtained.

The obtained results apply to the case of an isolated target, however they can be easily extended to the case of an illuminated area. Accounting for the azimuth spot dimension X, the maximum azimuth signal extension after the first compression step in (12) is given by

$$\begin{aligned}
X_s &\approx \max\left(\frac{\lambda \tilde{r}}{L} + X_I \frac{|r - \tilde{r}|}{r}\right) \\
&\le \frac{\lambda r_M}{L} + X_I \frac{|r_M - r_m|}{r_m} \quad \text{with } X < X_s < X_I.
\end{aligned} \tag{15}$$

The inequality $X_S < X_I$ in (15) is generally satisfied for typical spotlight configurations thus allowing to consider the convolution operation shown in (12) as a bulk azimuth compression step which reduces the azimuth signal extension from X_I to X_s.

B. Efficient Implementation in the Discrete Domain

Let us now investigate the discrete domain implementation of (12); this is particularly relevant due to the sampling operation carried out on the received raw signal. We start by computing the result of the bulk azimuth compression by setting the following output azimuth pixel spacing:

$$\Delta x'' = \frac{1}{W \xi_S} = \frac{\Delta x'}{W} \tag{16}$$

[3]Generalization to those cases where SPM cannot be applied can be derived as in [19]. Here we are interested only in having a rough measure of the target echo extension following the first processing step.

with $W \geq V$, i.e., with a pixel spacing satisfying the Nyquist limit of the spotlight signal, see (8) and (9). Accordingly, similarly to what is shown in the continuous analysis presented in the previous section, (12) becomes

$$\begin{aligned}\overline{a}(n\Delta x'', x, r) &= \sum_{i=-R/2}^{R/2-1} a(i\Delta x', x, r)s(n\Delta x'' - i\Delta x') \\ &= \exp\left[j2\pi \frac{(n\Delta x'')^2}{\lambda \tilde{r}}\right] \sum_{i=-R/2}^{R/2-1} a(i\Delta x', x, r) \\ &\quad \times \exp\left[j2\pi \frac{(i\Delta x')^2}{\lambda \tilde{r}}\right] \exp\left[-j2\pi \frac{2\Delta x' \Delta x''}{\lambda \tilde{r}} in\right] \\ &\quad \text{with } n = -B/2, \ldots, B/2 - 1 \end{aligned} \tag{17}$$

wherein $R = X_I/\Delta x'$ is the azimuth raw signal pixel number, and $B = round(X_s/\Delta x'')$ is the output data set azimuth extension $round(.)$ being the nearest integer operator. Note that, due to (10), R and B are on the same order. Moreover, the last exponential factor in (17) has the form of an FT kernel. In order to use FFT codes and avoid the employment of less efficient scaled FT (SCFT) codes [12], [15], we can exploit the freedom degree in the selection of $\tilde{r}$. Accordingly let us set $\tilde{r}$ as follows:

$$\frac{\lambda \tilde{r}}{2\Delta x'} = P\Delta x'' \geq X_s \quad \text{with } P \in N \tag{18}$$

where the factor $P\Delta x''$ represents the output azimuth data replication. Accordingly, under the validity of the inequality in (18), not only the azimuth spectral folding effects are avoided, see (16), but also no data wrap around occurs in the azimuth direction. We note that the validity of the aforementioned inequality in (18) is generally satisfied due to the presence of a slight azimuth data oversampling carried out on the spotlight signal with respect to the Nyquist rate that we would have with the system operating in the stripmap mode. This point can be clarified by accounting for (15) in the inequality in (18). In this case, we get

$$\frac{L/2}{\Delta x'} \geq 1 + \max\left(\frac{X_I \dfrac{|r - \tilde{r}|}{r}}{\lambda \tilde{r}/L}\right). \tag{19}$$

The quantity at the left-hand side of (19) is the ratio between the Nyquist limit of the stripmap acquisition ($L/2$) and the raw data pixel spacing ($\Delta x'$). This ratio, due to a typical 20–30% oversampling with respect to the Nyquist limit of the stripmap mode, is on the order of $1.2 \div 1.3$. Accordingly, the inequality in (18) is satisfied by setting $\tilde{r}$ such that

$$\max\left(\frac{|r - \tilde{r}|}{\tilde{r}r}\right) \leq \frac{\lambda}{LX_I}\left[\frac{L/2}{\Delta x'} - 1\right]. \tag{20}$$

Note that the requirement in (20) is fulfilled for any value of $\tilde{r}$ within (r_m, r_M) if

$$\frac{r_M - r_m}{r_M r_m} \leq \frac{\lambda}{LX_I}\left[\frac{L/2}{\Delta x'} - 1\right]. \tag{21}$$

For instance, a 20% of oversampling and a spot acquisition length (X_I) such that $X_I \approx 5X$ gives a value of about $5 \times 0.2 \times 1/r_M$ for the right-hand side factor in (21). This leads to the new inequality $r_M - r_m \leq 0.1 r_m$, which is satisfied for most real spotlight SAR systems.

Of course in the (rare) case of an insufficient oversampling factor, a balancing choice would be represented by setting $\tilde{r}$ at the midrange swath, thus leading to a resolution degradation at the image near and far range edges. Anyway, we remark that this is generally not a very critical issue because, due to the antenna beam steering, those targets would be in any case characterized by a lower resolution [10].

Based on (18), we can finally rewrite (17) as follows:

$$\begin{aligned}\overline{a}(n\Delta x'', x, r) &= \exp\left[j2\pi \frac{(n\Delta x'')^2}{\lambda \tilde{r}}\right] \sum_{i=-P/2}^{P/2-1} a(i\Delta x', x, r) \\ &\quad \times \exp\left[j2\pi \frac{(i\Delta x')^2}{\lambda \tilde{r}}\right] \exp\left[-j2\pi \frac{in}{P}\right] \\ &= \exp\left[j2\pi \frac{(n\Delta x'')^2}{\lambda \tilde{r}}\right] \\ &\quad \times \text{DFT}\left[a(i\Delta x', x, r) \exp\left[j2\pi \frac{(i\Delta x')^2}{\lambda \tilde{r}}\right]\right] \\ &\quad \text{with } n = -P/2, \ldots, P/2 - 1 \end{aligned} \tag{22}$$

wherein the DFT[.] symbol represents the discrete FT operator.[4] Note that having a degree of freedom in setting $\tilde{r}$, see the considerations about (22), a smart choice would be to select $\tilde{r}$ such that $P(\neq R)$ allows the use of efficient FFT codes. In this case, being P of the order of R [see (10)], a limited zero padding of the raw data $a(.)$ is required and implemented via the substitution

$$\sum_{i=R/2}^{R/2-1} \cdot \rightarrow \sum_{i=P/2}^{P/2-1} \cdot .$$

It is evident from (22) that we have obtained an output pixel spacing satisfying the Nyquist limit shown in (8) and (9) and, at the same time, we have achieved a very efficient implementation of the bulk azimuth compression step of (12).

We further remark that, until now, we have assumed the absence of any squint angle. Should this assumption not be valid, two main effects can be induced. The first effect is an azimuth wrap around of the data obtained after the convolution operation implemented in (12). This is not a difficult problem because a proper azimuth linear phase term could be included in the function $s(.)$ in (11) [and equivalently in (17)] to compensate for this effect. Secondly, due to the appearance of a significant range walk effect [15] in the RCM, an additional edge degradation could appear even at midrange. Although the paper is focused on low squint angle acquisitions, we stress that well known procedures applied for mitigating the range walk effect in deramping-based focusing approaches could be considered [20]. However, this is worth pursuing for future studies.

[4]Note also that, at variance with what is shown in (22), a more conventional expression of the DFT operation can be considered implying $\sum_{i=0}^{P-1} \cdot$ with $n = 0, \ldots, P-1$ instead of $\sum_{i=P/2}^{P/2-1} \cdot$ with $n = -P/2, \ldots, P/2 - 1$ [18]. In this case, a trivial manipulation of (22) is required.

IV. Residual Data Focusing via Stripmap Processing Techniques

Let us concentrate on the result of the bulk azimuth compression step shown in (12). We underline that, following this operation, the folding effect influencing the azimuth spectrum is avoided and the space-variant characteristics of the system transfer function are maintained. Accordingly, it is possible to carry out the residual focusing of the data via the use of efficient and precise techniques originally designed for stripmap SAR data focusing that are implemented in the frequency domain.

To clarify this point, we refer to the expression of the received signal over a distributed scene by resorting the linearity of the system

$$h(x', r') = \iint dx\, dr \gamma(x, r) g(x' - x, r' - r, x, r) \tag{23}$$

$$g(x' - x, r' - r, x, r) = \exp\left[j \frac{4\pi}{\lambda} r \right] f(x' - x, r' - r, x, r) \tag{24}$$

where $\gamma(x, r)$ represents the reflectivity function of the illuminated scene including the fast varying phase term in (24). The received data spectrum can be written as follows:

$$\begin{aligned} H(\xi, \eta) &= \iint dx'\, dr' h(x', r') \exp[-j2\pi\xi x'] \\ &\quad \times \exp[-j2\pi\eta r'] \\ &= \iint dx\, dr \gamma(x, r) \exp[-j2\pi\xi x] \\ &\quad \times \exp[-j2\pi\eta r] G(\xi, \eta, x, r) \end{aligned} \tag{24}$$

where η is the range (spatial) frequency, and $G(\cdot)$ is the spotlight SAR system transfer function (STF)

$$\begin{aligned} G(\xi, \eta, x, r) = \iint dx'\, dr' g(x' - x, r' - r, x, r) \\ \times \exp[-j2\pi\xi(x' - x)] \exp[-j2\pi\eta(r' - r)]. \end{aligned} \tag{26}$$

The expression of $G(\cdot)$ can be found via the application of the SPM, leading to the following expression [15]:

$$H(\xi, \eta) \approx G_0(\xi, \eta) \Gamma(\xi, \eta\Omega(\xi) + \mu(\xi)) \tag{27}$$

where

$$\begin{aligned} G_0(\xi, \eta) &= \exp\left[j \frac{\pi^2}{2\alpha/c^2} \eta^2 \right] \\ &\quad \times \exp\left[-j2\pi r_0 \left(\sqrt{\left(\frac{2}{\lambda} + \eta \right)^2 - \xi^2} - \left(\frac{2}{\lambda} + \eta \right) \right) \right] \end{aligned} \tag{28}$$

is the space invariant component of the SAR STF matched to the scene middle range r_0, $\Gamma(\xi, \eta)$ is the FT of $\gamma(x, r)$, and $\Omega(\xi)$ and $\mu(\xi)$ are two functions that describe the space-variant characteristics of the SAR STF associated with the RD RCM effect and to the range variation of the azimuth chirp rate usually referred to as focus depth (FD). This effect is known as Stolt mapping [11] or grid deformation [21]. The expressions of $\Omega(\xi)$ and $\mu(\xi)$ can be found in [15]. The key point in this context is to note that precise and efficient codes compensating for the Stolt mapping are available within the frame of stripmap SAR processing techniques but their application is allowed only in the absence of spectral folding effects. This rarely occurs when dealing with spotlight mode SAR systems.

Let us now consider the spectrum of the spotlight signal following the bulk azimuth compression step, for example $h_s(\cdot)$. In this case, we have

$$\begin{aligned} H_s(\xi, \eta) &= \mathrm{FT}[h_s(\cdot)] \\ &= \mathrm{FT}[h(\cdot) \otimes_{\mathrm{az}} s(\cdot)] \\ &= H(\xi, \eta) \exp\left[-j2\pi \frac{\xi^2 \lambda \tilde{r}}{4} \right] \end{aligned} \tag{29}$$

wherein the phase factor $\exp[-j2\pi\xi^2\lambda\tilde{r}/4]$ accounts for the bulk compression step. By finally substituting (27) in (29), we get

$$\begin{aligned} H_s(\xi, \eta) &= \exp\left[-j2\pi \frac{\xi^2 \lambda \tilde{r}}{4} \right] \\ &\quad \times G_0(\xi, \eta) \Gamma[\xi, \eta\Omega(\xi) + \mu(\xi)] \\ &= \overline{G}_0(\xi, \eta) \Gamma[\xi, \eta\Omega(\xi) + \mu(\xi)] \end{aligned} \tag{30}$$

with

$$\overline{G}_0(\xi, \eta) = \exp\left[-j2\pi \frac{\xi^2 \lambda \tilde{r}}{4} \right] G_0(\xi, \eta). \tag{31}$$

We explicitly note that the spotlight spectrum expression in (31) formally differs from that of the stripmap raw signal only for the presence of the function $\overline{G}_0(\cdot)$ instead of $G_0(\cdot)$ [15]. Moreover, the folding effects influencing the azimuth raw signal spectrum (see Section II) have been avoided due to the already carried out bulk azimuth compression step leading to the new pixel spacing $\Delta x''$ shown in (18). We also note that the space-variant characteristics of the system transfer function are preserved by the bulk compression. This nonlinear mapping of the range frequencies, i.e., $\eta\Omega(\xi) + \mu(\xi)$ in the reflectivity spectrum expression, is the same in (30) and (27).

Accordingly, precise and efficient stripmap focusing techniques, implemented in the frequency domain via FFT codes, can be applied to carry out the residual focusing of $h_s(\cdot)$ by simply accounting for the system transfer function component $\overline{G}_0(\cdot)$ instead of $G_0(\cdot)$ and by considering the new azimuth sampling frequency.

In particular, we have considered the stripmap processing approach described in [12], and the overall processing block diagram is shown in Fig. 2. In this case, the first step carries out the bulk azimuth compression, while the residual focusing is implemented as follows: the filtering operation, carried out in the two-dimensional (2-D) frequency domain via the filter function $\overline{G}_0^*(\cdot)$ allows us to fully focus the midspot area by accounting

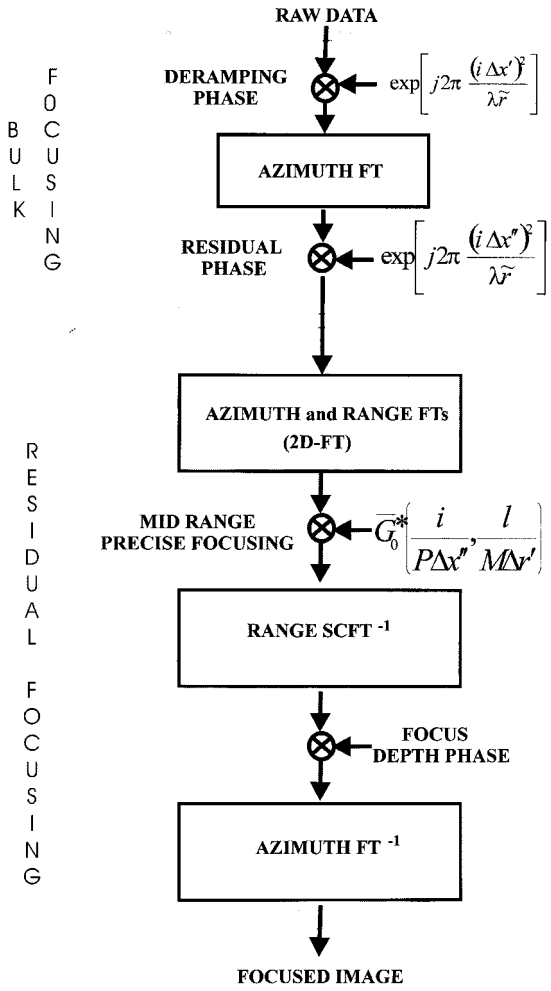

Fig. 2. Two-step focusing procedure block diagram. Note that $i = -P/2, \ldots, P/2-1$ and $l = -M/2, \ldots, M/2-1$. Moreover, $1/(P\Delta x'')$ and $1/(M\Delta r')$ represent the azimuth and range spectral samples dimensions, respectively.

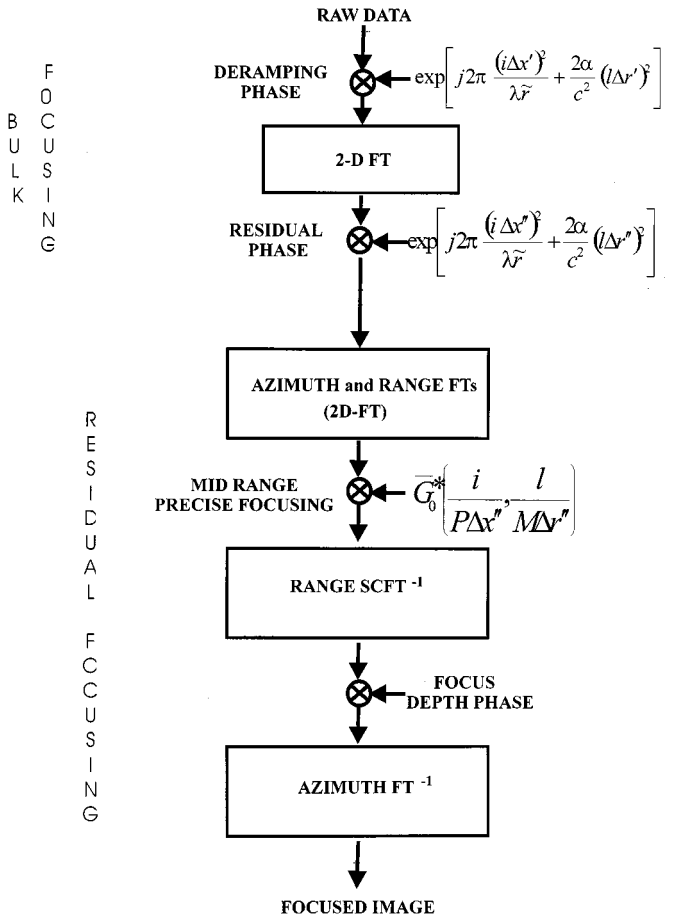

Fig. 3. Block diagram of the two-step focusing procedure in presence of high bandwidth transmitted signals. Note that $i = -P/2, \ldots, P/2-1$ and $l = -M/2, \ldots, M/2-1$. Moreover, $1/(P\Delta x'')$ and $1/(M\Delta r'')$ represent the azimuth and range spectral samples dimensions, respectively.

for all the effects that have not been considered during the first bulk processing step. In particular, it implements the range compression, the range migration compensation at mid swath and accounts for the residual azimuth compression operation. The range SCFT^{-1} operation, and the focus depth compensation steps take care for the $\Omega(\xi)$ and $\mu(\xi)$ terms of (30), respectively. We explicitly note that no approximations are present in the processing procedure in Fig. 2, which easily extends the focusing capability of a standard stripmap processing algorithm to the spotlight data. We also note that the proposed approach is computationally efficient because it does not require any significant increase of the raw data matrix dimensions and only involves matrix multiplication and FFTs. Finally, it is evident that, instead of procedure [12], alternative stripmap approaches, for example, those presented in [11], [13], [22], can be applied to carry out the residual focusing operation without any relevant impact on the proposed two-step processing approach.

A. Residual Data Focusing in Presence of High Bandwidth Transmitted Chirps

In the previous analysis, we have implicitly assumed that the received raw signal is sampled in the range direction with a frequency which satisfies the Nyquist limit imposed by the transmitted chirp bandwidth. However, as already mentioned, chirp signals with large bandwidths are often used in the spotlight case in order to equalize azimuth and range resolutions. These large bandwidths are often achieved by transmitting pulses with a spatial duration larger than the range extension of the illuminated spot referred hereafter to as Δr. In this case, significant data rate reduction can be obtained by sampling the received echoes with the frequency

$$f_p = \Delta f \frac{\Delta r}{c\tau/2} < \Delta f \quad \text{with } \Delta r/(c\tau/2) < 1. \tag{32}$$

Likewise, in the azimuth case, a selection of the sampling frequency according to (32) allows reducing the data rate but causes a range spectral folding effect that inhibits the use of frequency-domain range compression techniques. In this case, the range compression operation can be implemented in a way that is very similar to that shown in the bulk focusing step of Fig. 2. In particular, if we assume the validity of the expressions (32) and consider the generic (sampled) expression of a received echo $h(l\Delta r')$ with $l = -S/2, \ldots, S/2-1$ [being $\Delta r' = c/(2f_p)$, and S is the number of samples for each echo], the

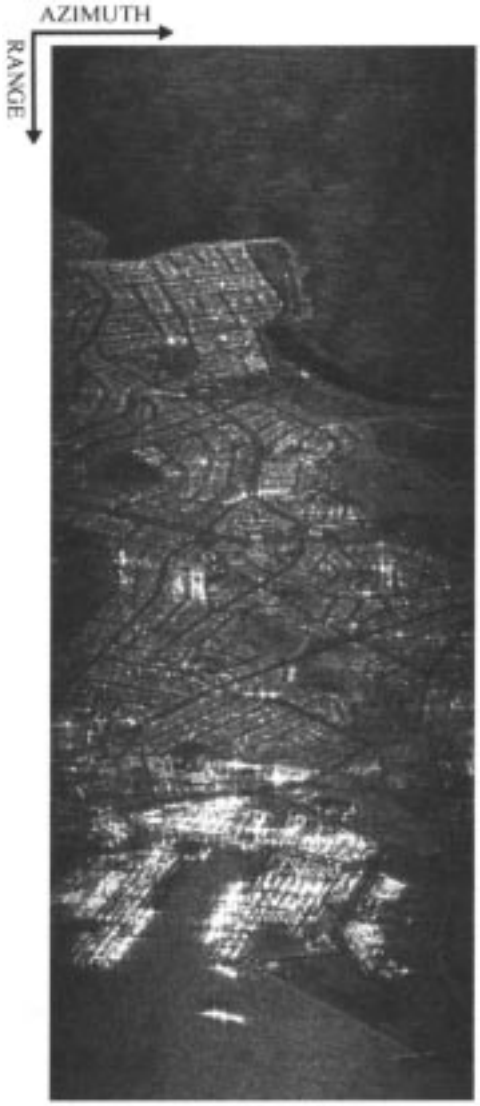

Fig. 4. C-band VV-polarized image of the Sidney zone obtained by applying the focusing approach of Fig. 5 to the raw data set acquired in 1994 by the SIR-C system operating in an experimental spotlight mode. The expected azimuth resolution is about 1 m, but the image is represented with an azimuth pixel spacing of about 6.5 m to avoid the geometric distortions caused by different dimensions of the pixel in range and azimuth directions. The extension of the area is of about 1.7 km × 4.5 km.

range compression of $h(.)$ can be carried out as follows [1], [2]:

$$\begin{aligned}\overline{h}(m\Delta r'') &= \exp\left[j\,\frac{2\alpha}{c^2}\,(m\Delta r'')^2\right] \\ &\quad\times \mathrm{DFT}\left[h(l\Delta r')\exp\left[j\,\frac{2\alpha}{c^2}\,(l\Delta r')^2\right]\right] \\ &= \exp\left[j\,\frac{2\alpha}{c^2}\,(m\Delta r'')^2\right]\sum_{l=-M/2}^{M/2-1} h(l\Delta r') \\ &\quad\times \exp\left[j\,\frac{2\alpha}{c^2}\,(l\Delta r')^2\right]\exp\left[-j\,\frac{2\pi}{M}\,lm\right] \\ &= \sum_{l=-S/2}^{S/2-1} h(l\Delta r')\exp\left[j\,\frac{2\alpha}{c^2}\,(l\Delta r'-m\Delta r'')^2\right], \\ &\qquad \text{with } m=-M/2,\ \ldots,\ M/2-1 \end{aligned} \tag{33}$$

TABLE I
SIR-C C-BAND SENSOR CHARACTERISTICS RELATIVE TO THE SAR IMAGES OF FIGS. 4–6

PARAMETER	VALUE	UNIT
MISSION	SRL-2	-
DATA	September 1994	-
SAR SYSTEM	SIR-C	-
ALTITUDE	222	Km
SWATH VELOCITY	7.26	Km/s
WAVELENGTH	0.0565816	m
POLARIZATION	VV	–
PULSE DURATION	8.4449854	μs
PULSE BANDWIDTH	20.0377808	MHz
COMPLEX SAMPLING RATE	22.4985600	MHz
QUANTIZATION	BPFQ	-
PRF	1620.	Hz
ECHO DELAY TIME	980.5416870	μs
RANGE BEAMWIDTH 3 dB	4.0867548	deg
AZIMUTH BEAMWIDTH 3dB	0.2694999	deg
ANTENNA LENGTH	12.1000004	m
ANTENNA WIDTH	0.7400000	m
LOOK ANGLE	42.2457428	deg
INCIDENCE ANGLE	44.1303482	deg
TOTAL (AZIMUTH) ANGULAR APERTURE (MID-RANGE)	1.6	deg
ORBIT DIRECTION	Descending	-
LOOKING DIRECTION	Right	-
PRF AMBIGUITY	1	-

where $\Delta r'' \le c/(2\Delta f)$ is the output range spacing satisfying the Nyquist limit imposed by the transmitted chirp bandwidth, and

$$M = \frac{\Delta r}{\Delta r''} = \frac{\pi c^2}{\alpha \Delta r' \Delta r''} \ge S \tag{34}$$

represents the number of samples of the range-compressed signal. It is easy to recognize in the last identity of (33) the matched filter operation implementing the range compression step, i.e., the convolution between the received signal $h(.)$ (zero padded to increase its extension from S to M) and the signal $d(l\Delta r') = \exp[j2\alpha(l\Delta r')^2/c^2]$. The latter represents the sampled expression of a chirp that has an inverted modulation rate with respect to the transmitted one and is symmetric to the range of the spot center at closest approach (which is constant for all the echoes). By comparing (22) and the first identity of (33), similarity between these two operations is evident.

Based on the above analysis, it is clear that in presence of high bandwidth transmitted chirps sampled according to (32), the processing algorithm sketched in Fig. 2 must be simply modified to include the range processing operation before carrying out the residual focusing step. Indeed, at this stage, the range bulk processing not only performs the range compression operation but also avoids the folding effect of the range spectrum due to the limited sampling frequency. Accordingly, the cascade of the range and bulk azimuth compression procedure in Fig. 3 eliminates any 2-D spectral folding effect. The residual focusing operation can be still carried out via the use of existing stripmap codes by simply considering the new expression of the function $\overline{G}_0(\cdot)$ in (31), becoming

$$\begin{aligned}\overline{G}_0(\xi,\eta) &= \exp\left[-j2\pi\,\frac{\xi^2\lambda\tilde{r}}{4}\right] \\ &\quad\times \exp\left[-j\,\frac{\pi^2}{2\alpha/c^2}\,\eta^2\right] G_0(\xi,\eta).\end{aligned} \tag{35}$$

This also includes the phase factor $\exp[-j\pi^2\eta^2/(2\alpha/c^2)]$ accounting for the range compression step already carried out.

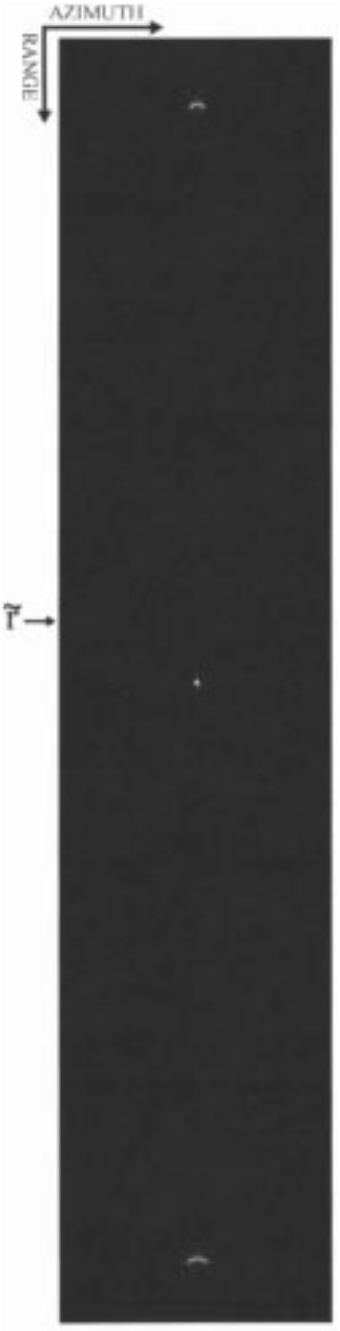

Fig. 5. Simulated image obtained after the bulk azimuth compression (range compression has been also implemented).The range corresponding to $\bar{r}$ is highlighted.

Fig. 6. Simulated image obtained by applying the focusing procedure of Fig. 2.

Clearly, although not explicitly mentioned, the range pixel spacing $\Delta r''$ resulting from the range focusing operation of (33) must also be considered for the implementation of the residual focusing step.

As final remarks, we underline that all the operations involved in (33) are assumed, in our case, to be carried out after the A/D conversion in the receiver. Moreover, the computational efficiency of the procedure in Fig. 3 can be further improved by combining the range compression operation and the compensation of the scaling factor $\Omega(\xi)$, which is carried out in the residual focusing step of Fig. 3 via the SCFT^{-1} operation. This result can be achieved by following the lines of the approach proposed in [10].

V. Experimental Results

In order to validate the presented theory, we have carried out a number of experiments. In particular, we have considered the raw data set relative to the Sydney area (Australia) acquired in

TABLE II
RESULTS OF THE ANALYSIS CARRIED OUT ON THE IMAGED POINT TARGETS OF FIG. 6

	Theoretical Near/Mid/Far range target	Near range target	Mid range target	Far range target	Unit
Azimuth resolution	0.907/0.919/0.932	0.913	0.924	0.937	m
Range resolution	6.587	6.597	6.591	6.593	m
Azimuth PSLR	-13.26	-13.26	-13.26	-13.26	dB
Range PSLR	-13.26	-13.26	-13.26	-13.26	dB
Azimuth ISLR	-10.11	-10.12	-10.11	-10.12	dB
Range ISLR	-10.11	-10.11	-10.11	-10.11	dB

1994 by the C-band sensor of the SIR-C system operated in the experimental spotlight mode (see Table I for a description of the system parameters). In this case, because of the ratio $f_p/\Delta f > 1$, see Table I, no spectral folding effect occurs in the range direction and therefore the applied focusing procedure is the one shown in Fig. 2.

We remark that in our case the azimuth raw data oversampling factor, i.e., $[L/(2\Delta x') - 1]$ is about 33%, $X_I \approx 7976$ m, the slant range extension of the scene is $\Delta r = 13.334$ km, and the near, mid, and far range distances are $r_m = 292.568$ km, $r_0 = 299.235$ km, and $r_M = 305.902$ km, respectively. The selected value of $\tilde{r}$ is $\tilde{r} = 298.821$ km. Accordingly, based on the analysis of Section III, we can evaluate the minimum and maximum range distance, for example r'_m and r'_M, which ensure the absence of degradation at the edges of the image, by using (20). They are given by

$$r'_m = 282.361 \text{ Km} < r_m$$

and

$$r'_M = 317.319 \text{ Km} > r_M \tag{36}$$

thus guaranteeing the possibility of focusing the overall scene. The image obtained by applying the procedure of Fig. 2 is presented in Fig. 4. It clearly shows the focusing capability of the proposed algorithm.

However, the absence of known reference targets in the scene does not allow any significant quantitative measurement of the quality of the obtained image. Accordingly, in order to assess the performance of the proposed approach, we have generated a simulated data set representing the signal backscattered by a sequence of three point targets aligned in the range direction and located over an absorbing background. The system parameters are again those of Table I.

To better clarify the effect of the bulk azimuth compression step, we show the result obtained by applying this operation (see Fig. 5). As expected, the achieved azimuth compression[5] effect is more relevant for the target located at a range closer to $\tilde{r}$. We additionally remark that the azimuth extension of the bulk compressed data is of 2048 samples, and it has been increased[6] with respect to the raw data, by about 20% (the azimuth raw data length was of 1700 samples), but no additional data dimension increase is required in the residual focusing step. Note also in Fig. 5 the effect of the uncompensated range cell migration effect.

[5]In order to improve the readability of the result, a range compression step has been also carried out.

[6]This allowed the use of high efficient FFT codes with a power of two data lengths [18].

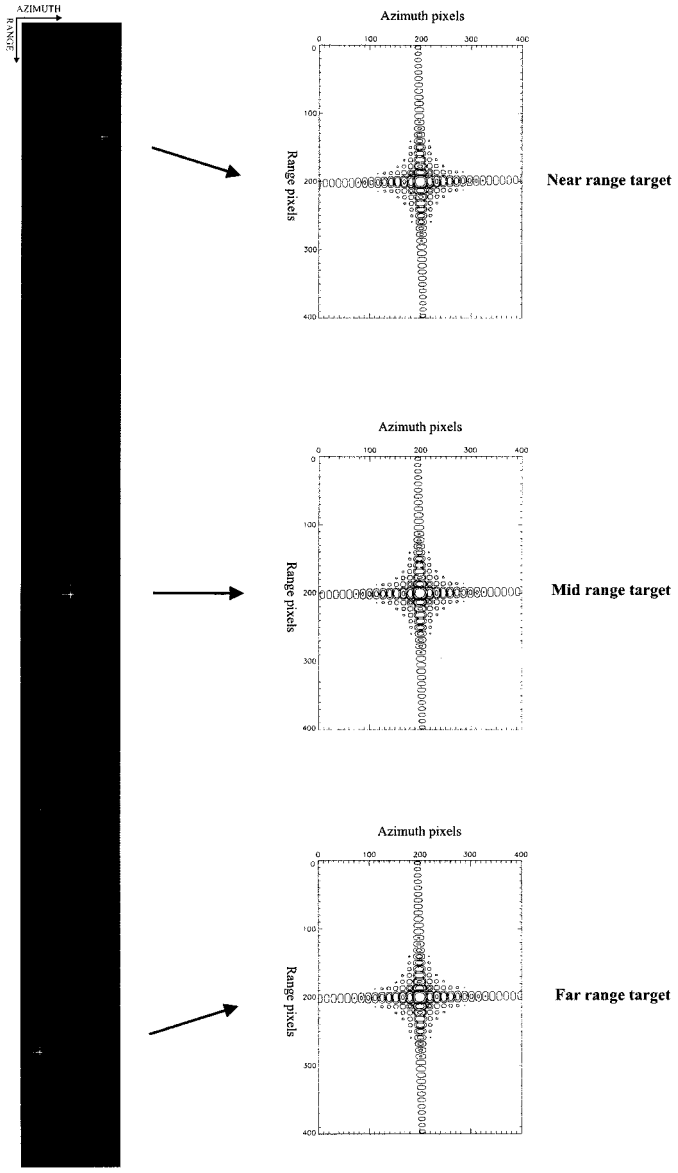

Fig. 7. High resolution simulated image obtained by applying the focusing procedure of Fig. 3. The contour plots of the three imaged point targets are also shown.

The fully focused image is finally shown in Fig. 6. The results of the measurements carried out on the imaged point targets of Fig. 6 are summarized in Table II wherein the theoretical azimuth resolution values are those pertinent to the selected point reflector. The inspection of Table II clarifies the high performance of the presented technique for what concerns the amplitude characteristics of the target responses. The phase accuracy has been also assessed; it is about 1°, thus demonstrating the phase preserving capability of the presented procedure.

In order to further investigate the performance of the proposed approach, we have also carried out a new simulation. It is again based on the sensor parameters of Table I, but now we have assumed a much higher transmitted signal bandwidth (140. MHz instead of 20. MHz), a nearly doubled range swath extension (21 km instead of 13 km), and a squint angle of about

TABLE III
RESULTS OF THE ANALYSIS CARRIED OUT ON THE IMAGED POINT TARGETS OF FIG. 7

	Theoretical Near/Mid/Far range target	Near range target	Mid range target	Far range target	Unit
Azimuth resolution	0.932/0.956/0.979	0.940	0.962	0.985	m
Range resolution	0.954	0.961	0.959	0.959	m
Azimuth PSLR	-13.26	-13.23	-13.26	-13.27	dB
Range PSLR	-13.26	-13.27	-13.27	-13.27	dB
Azimuth ISLR	-10.11	-10.14	-10.13	-10.18	dB
Range ISLR	-10.11	-10.17	-10.13	-10.15	dB

1°. Note that also in this case, three targets placed at near, mid, and far range, over an absorbing background, have been assumed. However, now the targets at near and far range have been placed close to the azimuth edges.

The result achieved in this case by applying the proposed focusing technique is shown in Fig. 7, while the results of the measurements carried out on the imaged targets are presented in Table III. Inspection of these results confirms the high precision focusing capability of the presented technique.

VI. CONCLUSIONS

A new algorithm for precise and efficient phase preserving focusing of spotlight data has been presented. It is based on a two-step approach that combines the efficiency of SPECAN algorithms with the precision of stripmap focusing techniques. The key point of the presented algorithm is an azimuth filtering step, efficiently carried out on the spotlight raw signal via a simplified version of the SPECAN procedure, which plays the role of a preprocessing stage. It allows the achievement of a bulk azimuth raw data compression and a pixel spacing smaller than (or equal to) the expected azimuth final resolution. Following this operation, a second processing step can be applied to carry out the residual focusing of the data via precise and efficient stripmap focusing procedures implemented in frequency domain and requires a minor modification.

This leads to a precise procedure, efficient and simple to implement, which easily extends the processing capability of standard stripmap procedures to spotlight data. Moreover, the application of the proposed approach to the case of high bandwidth transmitted chirp signals with a spatial extension larger than the range dimension of the illuminated spot, is shown to be straightforward. Experiments carried out on simulated and real data acquired in 1994 by the C-band spaceborne sensor of the SIR-C system operated in the experimental spotlight mode demonstrate the validity of the approach. The extension of the proposed focusing procedure to the data acquired in the hybrid stripmap/spotlight mode proposed in [23] is at the moment under study.

ACKNOWLEDGMENT

The authors would like to thank Dr. A. M. Guarnieri and the anonymous reviewers for their valuable comments and J. Corvino for proofreading the manuscript.

REFERENCES

[1] W. G. Carrara, R. S. Goodman, and R. M. Majewski, *Spotlight Synthetic Aperture Radar: Signal Processing Algorithms*. Norwood, MA: Artech House, 1995.
[2] C. V. Jakowatz, D. Wahl, P. Eichel, D. C. Ghiglia, and P. A. Thompson, *Spotlight-Mode Synthetic Aperture Radar: A Signal Processing Approach*. Norwell, MA: Kluwer Academic, 1996.
[3] D. C. Munson, Jr., J. D. O'Brien, and W. K. Jenkins, "A tomographic formulation of spotlight mode synthetic aperture radar," *Proc. IEEE*, vol. 71, pp. 917–925, 1983.
[4] D. L. Mensa, S. Halevy, and G. Wade, "Coherent doppler tomography for microwave imaging," *Proc. IEEE*, vol. 71, pp. 254–261, 1983.
[5] M. Desai and W. Jenkins, "Convolution backprojection image reconstruction for spotlight mode synthetic aperture radar," *IEEE Trans. Image Processing*, vol. 1, pp. 505–517, May 1992.
[6] W. Ye, T. S. Yeo, C. B. Zhang, and Y. H. Lu, "Correction of geometric distortion in spotlight synthetic aperture imagery," *Int. J. Remote Sensing*, vol. 20, pp. 979–992, 1999.
[7] C. Prati, A. M. Guarnieri, and F. Rocca, "Spot mode SAR focusing with the $\omega - K$ technique," in *Proc. Int. Geoscience and Remote Sensing Symp.'91*, Helsinki, Finland, 1991.
[8] R. Lanari, P. Franceschetti, M. Tesauro, and E. Sansosti, "Spotlight SAR image generation based on strip mode focusing techniques," in *Proc. Int. Geoscience and Remote Sensing Symp.'99*, Hamburg, Germany, 1999.
[9] M. Y. Jin, "High quality spotlight SAR processing algorithm designed for LightSAR mission," in *Proc. Int. Geoscience and Remote Sensing Symp.'97*, Singapore, 1997.
[10] J. Mittermayer, A. Moreira, and O. Loffeld, "Spotlight SAR data processing using the frequency scaling algorithm," *IEEE Trans. Geosci. and Remote Sensing*, vol. 37, pp. 2198–2214, Sept. 1999.
[11] C. Cafforio, C. Prati, and F. Rocca, "SAR data focussing using seismic migration techniques," *IEEE Trans. Aerosp. Electron. Syst.*, vol. 27, pp. 194–207, 1991.
[12] R. Lanari, "A new method for the compensation of the SAR range cell migration based on the chirp Z-transform," *IEEE Trans. Geosci. Remote Sensing*, vol. 33, pp. 1296–1299, Mar. 1995.
[13] R. K. Raney, H. Runge, R. Bamler, I. G. Cumming, and F. H. Wong, "Precision SAR processing using chirp scaling," *IEEE Trans. Geosci. Remote Sensing*, vol. 32, pp. 786–799, July 1994.
[14] M. Sack, M. R. Ito, and I. G. Cumming, "Application of efficient linear FM matched filtering algorithms to synthetic aperture radar processing," *Proc. Inst. Elect. Eng.*, pt. F, vol. 132, pp. 45–57, 1985.
[15] G. Franceschetti and R. Lanari, *Synthetic Aperture Radar Processing*. Boca Raton, FL: CRC, 1999.
[16] R. K. Raney, "Doppler properties of radar in circular orbits," *Int. J. Remote Sensing*, vol. 7, pp. 1153–1162, 1986.
[17] K. Eldhuset, "A new fourth-order processing algorithm for spaceborne SAR," *IEEE Trans. Aerosp. Electron. Syst.*, vol. 34, pp. 824–835, July 1998.
[18] A. V. Oppenheim and R. W. Shafer, *Digital Signal Processing*. Englewood Cliffs, NJ: Prentice-Hall, 1975.
[19] A. W. Rihaczek, *Principles of High Resolution Radar*. New York: McGraw-Hill, 1969.
[20] J. C. Curlander and R. N. McDonough, *Synthetic Aperture Radar Systems and Signal Processing*. New York: Wiley, 1991.
[21] G. Franceschetti, R. Lanari, V. Pascazio, and G. Schirinzi, "WASAR: A wide-angle SAR processor," *Proc. Inst. Elect. Eng.*, vol. 139, pp. 107–114, 1992.
[22] M. Jin and C. Wu, "A SAR correlation algorithm which accommodates large range migration," *IEEE Trans. Geosci. Remote Sensing*, vol. GE–22, pp. 592–597, Nov. 1984.
[23] D. P. Belcher and C. J. Baker, "High resolution processing of hybrid stripmap/spotlight mode SAR," *Proc. Inst. Elect. Eng.*, vol. 143, pp. 366–374, 1996.

Riccardo Lanari (M'91–SM'01) received the degree (summa cum laude) in electronic engineering from the University of Napoli, "Federico II" Napoli, Italy, in 1989.

Since 1994, he has been with the Istituto di Ricerca per l'Elettromagnetismo ed I Componenti Elettronici (IRECE), National Research Council (CNR), where he is currently a Full Researcher. He is also an Adjunct Professor with the University of Sannio, Benevento, Italy. He has been a Visiting Scientist with

different foreign research institutes such as the Institute of Space and Astronautical Science (ISAS), Tokyo, Japan, the German Aerospace Research Establishment (DLR), Oberpfafenhoffen, Germany, and the Jet Propulsion Laboratory (JPL), Pasadena, CA, where he received a NASA recognition for the innovative development of a ScanSAR processor for the SRTM mission. His main research activities are in the SAR data processing field as well as in IFSAR techniques. On this topic, he has authored 30 international journal papers and, more recently, a book *Synthetic Aperture Radar Processing* (Boca Raton, FL: CRC). He also holds two patents on SAR raw data processing techniques.

Dr. Lanari has been Chairman at several international conferences and was invited to join the technical program committee for the IGARSS Conference in 2000 and 2001.

Manlio Tesauro received the Laurea degree (summa cum laude) in electronic engineering and the Ph.D. degree in electronic engineering and computer science, both from the University of Napoli "Federico II," Napoli, Italy, in 1992 and 1998, respectively.

In 1998 and 1999, he was with the Istituto di Ricerca per l'Elettromagnetismo ed I Componenti Elettronici (IRECE), Napoli, National Research Council (CNR), with a grant from Telespazio. Since 2000, he has been a Research Scientist with the Dipartimento di Ingegneria dell'Innovazione, University of Lecce, Lecce, Italy. In February 2000, he was a member of the Italian Team in the ASI Ground Data Processing Chain during the Shuttle Radar Topography Mission (SRTM) at the Jet Propulsion Laboratory, Pasadena, CA. His main interests are in the field of statistical signal processing with emphasis on SAR and IFSAR processing.

Eugenio Sansosti (M'96) received the Laurea degree (summa cum laude) in electronic engineering from the University of Napoli "Federico II," Napoli, Italy, in 1995.

Since 1997, he has been with the Istituto di Ricerca per l'Elettromagnetismo e I Componenti Elettronici (IRECE), National Research Council (CNR), where he currently holds a Full Researcher position. He is also an Adjunct Professor of electrical Communications at the University of Cassino, Cassino, Italy. He was a Guest Scientist with the Jet Propulsion Laboratory, Pasadena, CA, from August 1997 to February 1998, and again in February 2000 in support of the NASA Shuttle Radar Topography Mission. In November and December 2000, he worked as an Image Processing Adviser at the Istituto Tecnologico de Aeronautica (ITA), Sao José dos Campos SP, Brazil. His main research interests are in airborne and spaceborne synthetic aperture radar (SAR) data processing, SAR interferometry, and differential SAR interferometry.

Gianfranco Fornaro received the Laurea degree in electronic engineering from the University of Napoli "Federico II," Napoli, Italy, in 1992, and the Ph.D. degree from the University of Rome "La Sapienza," Rome, Italy, in 1997.

He is currently a Full Researcher at the Istituto di Ricerca per l' Elettromagnetismo e i Componenti Elettronici (IRECE), Italian National Research Council (CNR) and Adjunct Professor of Communication, University of Cassino, Cassino, Italy. He has been a Visiting Scientist with the German Aerospace Establishment (DLR), Oberpfafenhoffen, Germany, and the Politecnico de Milano, Milano, Italy, and has been a Lecturer with the Istituto Tecnologico de Aeronautica (ITA), Sao José dos Campos SP, Brasil. His main research interests are in the signal processing field with applications to the synthetic aperture radar (SAR) data processing, SAR interferometry, and differential SAR interferometry.

Dr. Fornaro was awarded the Mountbatten Premium Award by the Institution of Electrical Engineers (IEE) in 1997.